

# Fermi polaron in atom-ion hybrid systems

Renato Pessoa,<sup>1</sup> S. A. Vitiello,<sup>2</sup> and L. A. Peña Ardila<sup>3,\*</sup>

<sup>1</sup>*Instituto de Física, Universidade Federal de Goiás - UFG, 74001-970 Goiânia, GO, Brazil*

<sup>2</sup>*Instituto de Física Gleb Wataghin, Universidade Estadual de Campinas - UNICAMP, 13083-970 Campinas, SP, Brazil*

<sup>3</sup>*School of Science and Technology, Physics Division, University of Camerino, Via Madonna delle Carceri, 9B - 62032 (MC), Italy*

(Dated: January 11, 2024)

Charged quasiparticles dressed by the low excitations of an electron gas, constitute one of the fundamental pillars for understanding quantum many-body effects in some materials. Quantum simulation of quasiparticles arising from atom-ion hybrid systems may shed light on solid-state uncharted regimes. Here we investigate the ionic Fermi polaron consisting of a charged impurity interacting with a polarized Fermi bath. Employing state-of-the-art quantum Monte Carlo techniques tailored for strongly correlated systems, we characterize the charged quasiparticle by computing the energy spectrum, quasiparticle residue, and effective mass, as well as the structural properties of the system. Our findings in the weak coupling regime agree with field-theory predictions within the ladder approximation. However, stark deviations emerge in the strongly interacting regime attributed to the vastly large density inhomogeneity around the ion, resulting in strong correlations for distances on the order of the atom-ion potential range. Moreover, we find a smooth polaron-molecule transition for strong coupling, in contrast with the neutral case, where the transition smoothens only for finite temperature and finite impurity density. This study may provide valuable insights into alternative solid-state systems such as Fermi exciton polarons in atomically thin semiconductors beyond the short-range limit.

*Introduction* – Impurities interacting with a quantum many-body environment lead to the formation of quasiparticles termed polarons as the mobile impurity entangles with virtual quantum excitations in the medium. The concept of a quasiparticle is one of the milestones in Landau’s Fermi-liquid theory [1–3], originally introduced by Landau and further developed by Pekar [4] in the context of electrons embedded in polar crystals. In a very different energy scale, the high level of controllability in ultra-cold degenerate quantum mixtures has theoretically and experimentally inspired the study of a quantum analog of the solid-state polaron. These quasiparticles arise from the interaction between individual impurities and the low-energy excitations of the quantum gas. Experimental realization of both Bose [5–9] and Fermi polarons [10–14] has been achieved using alkaline atomic species employing spectroscopy and interferometric protocols to characterize these quasiparticles in cold atoms-setups [15].

Cold ion-atom hybrid systems, on the other hand, have emerged as a robust field at the crossroads of two well-consolidated fields, ultracold quantum gases and ion-trapped systems, offering potential and promising applications in quantum technologies, particularly quantum sensing, quantum computation as well as in quantum simulation [16]. In this context, combining quantum impurities and atom-ion hybrid systems may provide a powerful platform to study the interaction between the low-energy excitations of electrons with ions, as in the original solid-state crystal scenario [17]. More importantly, due to the hierarchy between the natural energy and length scales between solid-state crystal and ultracold atomic systems, impurities in hybrid atoms-ion systems serve as a testbed for currently unattainable regimes in solid-state [18]. Despite the extensive theoretical and experimental work on polarons in ultracold quantum gases, the degeneracy realm for the atom-ion mixture is still unreachable within current technology [19]. Nonetheless, tremendous efforts

are dedicated to coherently manipulating ions in degenerate quantum matter. For example, one of the big challenges is micro-motion; ions interacting with stray electric fields can lead to high-frequency motion of the ion. The energy scale associated with this oscillation is inherently related to its averaged kinetic energy and is mitigated by using different sophisticated experimental tricks [20, 21]. However, the charged impurity case offers advantages in transport studies with respect to its neutral counterpart, as demonstrated by employing external electric fields to investigate ionic impurity transport [22]. These techniques hold promise for exploring polaron properties, including effective mass and non-trivial transport properties, in the quantum degenerate regime. In addition, spatial and temporal correlation in polarons can be traced with high precision using a recent state-of-the-art ionic microscope [23]. This technology may enable access to the polaron size and the correlation between ions and atoms, allowing us to track the complicated out-of-equilibrium polaron dynamics [9, 24, 25]. The recent experimental capability to manipulate the atom-ion scattering length through Feshbach resonances [26] has triggered extensive theoretical investigations of impurities [27–29], and polarons in hybrid atom-ion systems, both in both Bose-Einstein condensates [30–32] and Fermi gases [32–34]. The key feature of this new polaronic flavor is the lack of length scale separation, given that the typical coherence length is comparable to the potential range. This implies that chemistry associated with few-body bound states may play a crucial role in the formation of many-body bound states or mesoscopic polarons [35]. As a result, in specific regimes, especially in the strongly correlated regime, the interplay between few and many-body physics cast in density deformations restraining the applicability of traditional techniques (which assume a fixed chemical potential for the medium) limited and, in some cases, ineffective. Thus, long-ranged polarons featuring large

backaction effects of the quantum medium in the presence of a strongly coupled impurity require *ab initio* techniques.

In this work, we study the ionic Fermi polaron problem using *ab initio* quantum Monte Carlo techniques. We characterize the polaron by computing its energy spectrum, effective mass, quasiparticle residue and the enhanced density extracted from the atom-ion pair correlation functions. In the regime of weak coupling, our results agree with both, the neutral Fermi polaron problem where a single excitation ansatz can be employed [36] and recent analytical approaches based on the ladder approximation. However, for strong interaction, the polaron properties change dramatically due to the density enhancement around the ion. Furthermore, the polaron-molecule transition exhibited in the neutral case also appears in our spectrum, yet the transition is continuous, which recently has been predicted for the neutral case [14] only for finite temperature and finite impurity density. Our numerical method includes the non-perturbative deformation of the bath and therefore, incorporates the non-trivial backaction effects needed for characterizing the polaron in the presence of strong interactions arising from the complex atom-ion potential.

*Model and Atom-ion interaction* – We investigate a scenario involving a single mobile ionic impurity with mass  $m_\downarrow$  and down spin, interacting with an oppositely spin-polarized, non-interacting Fermi gas of mass  $m_\uparrow$  at zero temperature, as illustrated in Fig. 1(a). The system is characterized by an *unperturbed* density, defined as Fermi gas density in the absence of the ion,  $n = N_\uparrow/V = (2m_\uparrow\epsilon_F/\hbar^2)/6\pi^2$ , where  $\epsilon_F$  is the Fermi energy. The Hamiltonian of the system is described by

$$\mathcal{H} = -\frac{\hbar^2}{2m_\downarrow}\nabla_\downarrow^2 + \sum_{i=1}^{N_\uparrow} \left[ -\frac{\hbar^2}{2m_\uparrow}\nabla_{\uparrow,i}^2 + V_{ai}(r) \right], \quad (1)$$

where the ion induces an atom-ion polarized potential [37] depending on the distance  $r = |\mathbf{r}_a - \mathbf{r}_i|$  from an atom to the ion, which can be described by the potential

$$V_{ai}(r) = -C_4 \frac{r^2 - c^2}{r^2 + c^2} \frac{1}{(r^2 + b^2)^2}. \quad (2)$$

The parameters  $b$  and  $c$  lock the potential depth and the effective repulsive short-range contribution, respectively. In addition, this pair is chosen to match the  $s$ -wave scattering length when solving the low-energy two-body problem. The strength of the potential is parameterized by  $C_4 = \alpha e^2/2$  which depends on the atomic static polarisability  $\alpha$  and  $e$  is the elementary electrostatic charge. The relevant length and energy scales are defined by the competition between the kinetic and the potential interaction range,  $r_\star = \sqrt{(2\mu C_4/\hbar^2)}$ , where  $\mu^{-1} = m_\downarrow^{-1} + m_\uparrow^{-1}$  is the reduced mass. The characteristic energy scale  $E^\star = \hbar^2/2\mu r_\star^2$  is proportional to the height of the centrifugal barrier for any partial wave

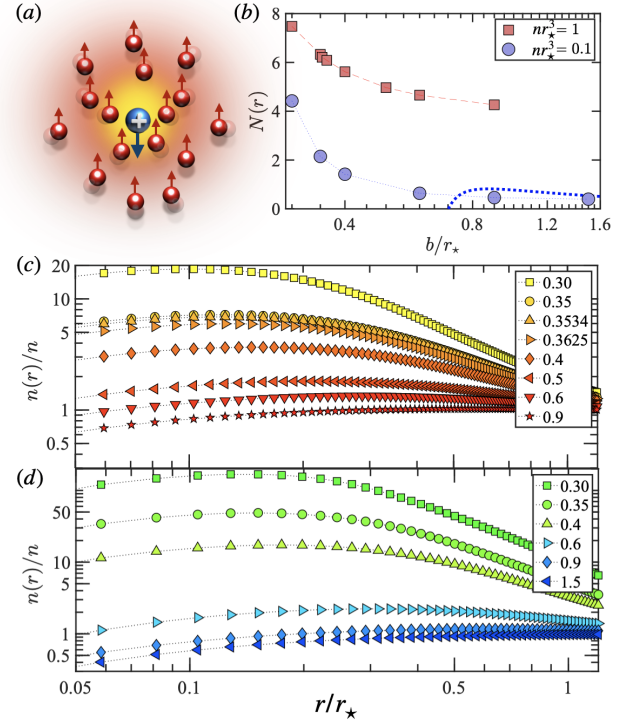


FIG. 1. (a) Ionic impurity  $\downarrow$  immersed in a polarized Fermi gas  $\uparrow$ . (b) Average number of fermions in the neighborhood of the ion enclosed in a sphere of radius  $r_\star$  for two unperturbed densities,  $nr_\star^3 = 1$  (red squares) and  $nr_\star^3 = 0.1$  (blue circles). The dotted blue line indicates the theoretical prediction for both the neutral Fermi polaron valid in the low-density regime and weak coupling,  $b \gg r_\star$  [12]. Density profile  $n(r)$  as a function of the distance at densities (c)  $nr_\star^3 = 1$  and (d)  $nr_\star^3 = 0.1$ , for different values of the parameter  $b$  of the atom-ion interaction. The lines connecting the points serve as visual guides.

and sets the upper bound for the energy for isotropic  $s$ -wave partial wave. For alkali atoms, the range of the potential is very small with respect to the interparticle distance, namely  $r_\star^0 \sim k_F^{-1} \ll n^{-1/3}$ , being  $k_F$  the characteristic Fermi vector. Due to this separation of length scales, a simple yet powerful variational wave function known as *Chevy* ansatz has been employed successfully to describe Fermi polarons with shorted-ranged interactions [36]. However, ion-atom hybrid systems differ vastly because they lack a hierarchy of length scales, bringing new polaronic effects with respect to the neutral case. In fact, for typical atom-ion mixtures, the range of the potential oscillates from  $1000a_0 < r_\star < 6000a_0$  [16], which may be on the same order as the interparticle distance and hence, finite-range effects become prominent, introducing a complex interplay between the few-body and many-body physics. Recently, range effects turned out to be relevant also in the neutral case [38]; however, the strong atom-ion potential can heavily modify the density of the host bath around the ion [31] and therefore, the ion polaronic properties are modified due to the redistribution of the density (see Fig. 1), which is also altered by the ion presence, leading to non-trivial backaction effects. Due to these two effects, our

aim in this work is to solve the many-body problem in Eq. (1) by using quantum Monte Carlo techniques, which have been proven to be a powerful state-of-the-art method for studying both neutral and charged quasiparticles.

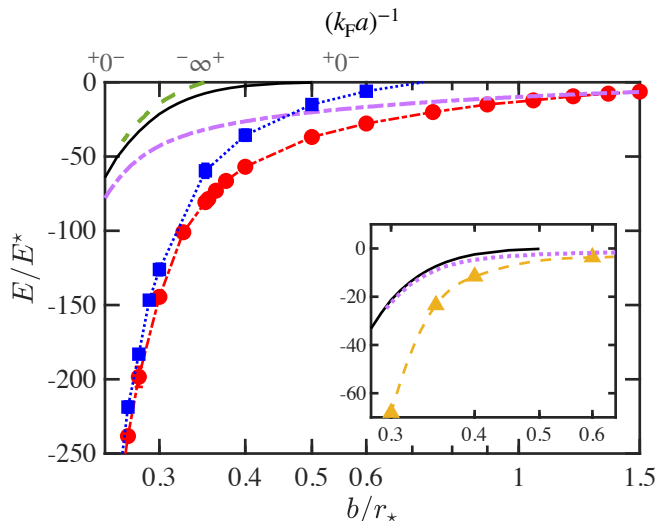


FIG. 2. Polaron energy  $E_p$  (red circles) and molecular energy  $E_M$  (blue squares) as a function of the parameter  $b$  and coupling strength  $(k_F a)^{-1}$  (upper scale) at the unperturbed density  $nr_*^3 = 1$ . Guidelines are included. Theoretical predictions using the ladder approximation by Christensen *et.al.* [33] are shown as a purple dash-dotted line for the polaron and a green dashed line for the molecule. Inset: Polaron energies (yellow triangles) at the unperturbed density  $nr_*^3 = 0.1$ . Ladder approximation polaron energy represented by a dotted purple line. The black continuous line depicts the solution for the atom-ion vacuum dimer.

*Quasiparticle properties* – We compute the many-body ground state of Eq. (1) as a function of the parameter  $b$  for a fixed  $c = 0.0023r_*$ . For slow impurities,  $\mathbf{p} \ll r_*^{-1}$ , the polaron energy is computed as  $E_p(\mathbf{p}) = \mu(\mathbf{p} = \mathbf{0}) + \mathbf{p}^2/2m^*$  where  $\mu = E^0(N_\uparrow, 1_\downarrow) - \frac{3}{5}N_\uparrow\epsilon_F$ , and  $E^0(N_\uparrow, 1_\downarrow)$  is the energy of the Fermi bath with an ion at zero momentum, while  $m^*$  is the effective mass. At the two-body level, we solve the low-energy two-body problem for the potential Eq. (S1) in the  $s$ -wave regime. The wavefunction’s asymptotic behavior at large distances provides the  $s$ -wave scattering length. In particular, for fixed  $c \ll r_*$  as in our case, the scattering length has an analytical form,  $a = \sqrt{b^2 + 1} \cot \left[ \pi/2 \frac{\sqrt{b^2 + 1}}{b} \right]$ . Thus, the two-body spectrum showcases several resonances as a function of  $b$ . The solution of the two-body problem enters in the explicit choice of the trial wave functions of the Jastrow-Slater form (see Supplemental Material).

Let us turn our attention to the energy spectrum at the many-body level. In Fig. 2, we plotted the polaron energy as a function of  $b$ . For values  $b \gtrsim 0.58r_*$  the two-body problem gives a scattering solution (no two-body bound state), whereas for  $0.26r_* \lesssim b \lesssim 0.58r_*$  the system admits a single two-body bound state. The energy of the vacuum two-body prob-

lem is represented by the black lines in Fig. 2. Instead, for values  $b \lesssim 0.26r_*$ , more resonances appear involving high-order few-body states. We focus on the regime leading up to forming one single-bound state to gain insight into the fundamental transition polaron-molecule. In the scattering regime,  $b \gtrsim 0.58r_*$  the polaron energy decreases as the resonance is approaching  $(k_F a)^{-1} = 0^-$ . Indeed, as the parameter  $b$  decreases, the potential depth increases, resulting in a more tightly bound polaron. This qualitative trend is followed by the ladder approximation approach as well [33], represented by the purple dashed-dotted line in Fig. 2. In addition, in the weakly interacting regime  $b > r_*$ , both theories agree quite well; however, strong quantitative deviations are observed as  $b$  decreases even further. The main reason for the discrepancy is associated with the high non-homogeneous density bath in the neighborhood of the ion that increases as  $b$  decreases. Note that neither backaction effects nor density deformations are fully considered in the ladder approximation. In Fig. 1(c), we compute the density around the ion and we observe large deviations from the unperturbed density  $n$  for length scales on the order of the potential range  $r < r_*$  for different values of  $b$ . Yet another intriguing scenario is at the low-density regime, namely  $nr_*^3 \ll 1$ . Due to the large separations of length scales, one expects to recover the physics of the neutral Fermi polaron at least for  $b \gg r_*$ . For both  $nr_*^3 = 0.1$  and  $b \gg r_*$  our simulations recover both the ladder approximation as well as the mean-field prediction  $E^{\text{MF}} = -\pi^2 \frac{n}{b} E^*$  [39]. Interestingly, even for the low densities and the regime where the atom-ion interaction matters,  $b \lesssim r_*$  deviations are displayed between QMC and the ladder approximation and become more evident as the resonance is approached. This comparison is shown in the inset of Fig. 2, revealing that even though the unperturbed density is small,  $nr_*^3 \ll 1$ , significant non-perturbative deviations are observed in the region  $r < r_*$ , for instance see Fig. 1(d).

In Fig. 2, another notable feature of the polaron emerges as an excited state when the resonance is crossed, the molecular branch. The nodal surface is built such that the ionic impurity is injected into the first momentum state above  $k_F$  and exciting one fermion to the corresponding state with opposite impurity momentum,  $\mathbf{k}$ , ensuring that the total impurity ion-fermion momentum remains zero. The molecular energies are computed with QMC and are represented by the blue squares in Fig. 2. The energy is computed by  $E_M = E^0(N_\uparrow - 1, 1_\uparrow^{k > k_F}, 1_\downarrow^{|-k| > k_F}) - \frac{3}{5}(N_\uparrow - 1)\epsilon_F$ , where  $E^0$  is the energy of the system with a molecule formed by the pair  $(1_\uparrow; 1_\downarrow)$  and the Fermi sea with  $N_\uparrow - 1$  atoms (see Supplemental material for a discussion on the molecular nodal surface). For a critical value  $b_c \simeq 0.37r_*$  or  $(k_F a)^{-1} \sim 1.28$ , the molecular branch meets the polaron state and becomes degenerate to the polaron branch. Akin to the polaron-molecule transition exhibited in the neutral case, the transition is pinpointed around  $(k_F a)^{-1} \sim 1.28$  [40]; however, for the values explored, our transition does not show any crossing, in contrast to the neutral, zero temperature and single impurity

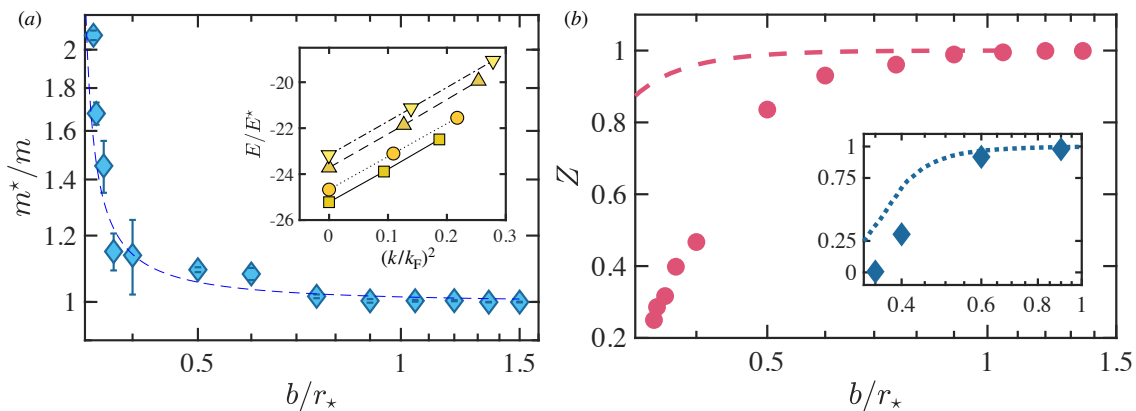


FIG. 3. **(a)** Effective mass of the ionic Fermi polaron as a function of the potential parameter  $b/r_*$  for  $nr_*^3 = 1$ . The inset presents the polaron energies as a function of the square momentum vector  $(k/k_F)^2$  for different numbers of particles in the bath  $N_\uparrow = 147$  ( $\blacksquare$ ), 123 ( $\bullet$ ), 93 ( $\blacktriangle$ ) and 81 ( $\blacktriangledown$ ). **(b)** Quasiparticle residue as a function of the potential parameter  $b/r_*$  for the density  $nr_*^3 = 1.0$ . The dashed and dotted lines are the theoretical results obtained by Christensen *et al.* [33]. The inset shows results at the density  $nr_*^3 = 0.1$ .

case, but instead the polaron-molecule transition is continuous presumably due to the long-range character of the atom-ion interactions and the choice of nodal surface. In the neutral case is argued that the nature of the first-order phase transition observed in the polaron-molecule is attributed to many-body correlations, while the transition disappears in the few-body limit [41]. Qualitatively, our result can be explained in terms of an effective potential. For  $b < 0.58$ , the ion experiences an effective potential consisting of a deep-ion potential supporting a two-body bound state and an additional potential arising from bath deformation. The latter mimics a microtrap potential, justified by the rapid increase in the effective mass of the ion (see Fig. 2). In other words, introducing an additional fermion attempting to occupy the two-body molecular state results in an energy increase due to the excess of the kinetic energy of the fermions and the Pauli exclusion; thus the effective potential becomes shallower than the bare potential, preventing the formation of higher-order bound states. Note that this effect arises due to highly local inhomogeneities of the impurity's density, as for example in the strongly attractive coupled Bose polaron [42] where the repulsion between bosons is played in our system by the Fermi Pauli blocking. In fact, in Fig. 1 (b) we found that the "molaron" is dressed by roughly  $N_\downarrow \approx 8$  fermions in the vicinity of the ion. The molecular branch energy presents notable differences against analytical approaches. Although the ladder approximation relies on a well-educated molecular ansatz, it only provides an upper bound for the molecule energy (see dashed green line in Fig. 2). In addition, QMC encompasses all possible correlations in the system, while the molecular ansatz for the ladder approximations is limited to low-order molecule-particle excitation.

In Fig. 3(a), we report the results for the effective mass of the ionic Fermi polaron as a function of the parameter  $b$ , for the fixed unperturbed density  $nr_*^3 = 1$ . In the weakly interacting regime  $b \gg r_*$ , the effective mass is slightly larger than one and increases as one approaches  $1/a = 0$ . On the

other hand,  $m^*$  is continuous when entering the two-body sector  $b \approx 0.58r_*$ . Both effects are consistent with the trend displayed by the polaron energy. As the system becomes more correlated, for values  $b < 0.58r_*$ , the effective mass grows rapidly. For  $b_c$ , the effective mass is roughly  $m^* \sim 2m$ , i.e. the mass of the bare ion-atom molecular pair. Indeed we find a finite effective mass in this regime, consistent with the molaron picture and the number of fermions in the dressed cloud. The rapid increase of the effective mass was also predicted using recent semiclassical approaches [34], however we do not expect any divergence from the range of parameters investigated. From a methodological standpoint, the polaron effective mass  $m^*/m$  is determined by calculating the dispersion energy of the polaron,  $E_p(\mathbf{p}) \approx \mu(\mathbf{0}) + \hbar^2 \mathbf{k}^2 / 2m^*$  as a function of  $(k/k_F)^2$ , where  $k$  is the ion's impurity wave vector, and then extrapolating for a larger number of particles in the thermodynamic limit (see Supplemental Material). The inset of Fig. 3 shows the fits for  $b/r_* = 0.6$  and  $N_\uparrow = 81, 93, 123$ , and 147 atoms; in fact, the linear behavior of the energies at low momentum demonstrates the reliability of the quasiparticle model.

Finally, we plotted in Fig. 3(b) the quasiparticle weight, which quantifies the difference between the polaron wave function with respect the initial non-interacting state. The residue is slightly smaller than one for  $b > r_*$ , namely the ion polaron resembles the non-interacting state. This result agrees with the ladder approximation by Christensen *et al.* [33] for high and low unperturbed densities,  $nr_*^3 = 1$  and  $nr_*^3 = 0.1$ , respectively. Nonetheless, for strong coupling and regardless of the density, the residue decays rapidly, approaching zero as one gets close to the first resonance  $1/a$ . This behavior is expected because the impurity gets more attracted to the atoms in the bath, and for a critical  $b_c$ , the molecule becomes the new ground state. Its wave function is orthogonal to the non-interacting initial state. For fixed  $b$ , a counterintuitive behavior was found first in [33] and

also corroborated by our numerical simulations in which the quasiparticle residue is smaller as the density increases. In our calculations for  $b = 0.35r_*$  the residue is  $Z \approx 0.25$  at the density  $nr_*^3 = 1$ , while for a smaller density, e.g.  $nr_*^3 = 0.1$  the residue drops to zero within statistical error. In fact, depending on the unperturbed density, the atom-ion potential can trap an average number of fermions as depicted in Fig. 1 (b). Indeed, for a fixed  $b$  the number of atoms trapped at high densities is larger than at lower densities. In the latter scenario, the ions interact with only a few fermions, resulting in relatively significant few-body effects rather than many-body, as illustrated in Fig. 2, where the energy of the dimer closely follows the one of the polaron, and therefore residue is notably large. Conversely, a sufficient number of fermions are present at higher densities, leading to collective local excitations that dress the ion, building up a tightly bound polaronic state characterized by a higher quasiparticle weight.

*Summary and outlook* – The ionic Fermi polaron quasiparticle is fully characterized by computing the energy spectrum, effective mass and quasiparticle residue using state-of-the-art quantum Monte-Carlo methods. In contrast to the neutral case, the long-range character of the atom-ion potential can effectively trap a large number of fermions that are effectively attracted by the ion, causing large deviations from the unperturbed density and, therefore, modifying the polaron properties heavily. In fact, our results quantitatively differ from the analytical approaches such as ladder approximation, for which the density is taken constant and the backaction effects are ignored. We also unveil a smooth polaron-molecule transition at zero temperature, starkly contrasting with the neutral case. The quasiparticle residue can be accessed by Raman spectroscopy with momentum-dependent measurements [14], while the effective mass can be extracted by diffusive transport of the ions as a function of an external electric field [43] or alternatively by measuring the low-lying compression modes [44] in the high imbalance atom-ion mixture trapped in a controllable Pauli trap. In the future, we plan to explore inducing interaction between Fermi ions polarons [45, 46]. Akin to the bosonic case [46], the strong density modulations might lead to strong pairing between ions due to induced interaction by the Fermi sea. Finally, an interesting avenue to pursue is to study excitonic polarons, which arise from the interaction of excitons and a Fermi gas in 2D [47, 48].

*Acknowledgments* – We thank G. Bruun, S. Giorgini, A. Camacho, K. Myśliwy, K. Jachymski and S. Pilati for insightful discussions. We thank E. Christensen for sharing his results in the ladder approximation. SAV acknowledges financial support from the Brazilian agency, Fundação de Amparo à Pesquisa do Estado de São Paulo grant #2023/07225-0, São Paulo Research Foundation (FAPESP). Computational resources have been provided in part by CENAPAD-SP at Unicamp. RP thanks the computer support from LaMCAD/UFG

and LAPA acknowledges financial support from PNRR MUR project PE0000023-NQSTI.

---

\* luis.penaardila@unicam.it

- [1] G. Baym and C. Pethick, [Landau Fermi-Liquid Theory](#) (Wiley, 1991-12).
- [2] Landau fermi-liquid theory and low temperature properties of normal liquid  $^3\text{He}$ , in [Landau Fermi-Liquid Theory](#) (John Wiley and Sons, Ltd, 1991) Chap. 1, pp. 1–121, <https://onlinelibrary.wiley.com/doi/pdf/10.1002/9783527617159.ch1>.
- [3] G. D. Mahan, [Many-particle physics](#), Physics of solids and liquids (Plenum, New York, NY, 1990).
- [4] L. Landau and S. Pekar, *Zh. Eksp. Teor. Fiz* **18**, 419 (1948).
- [5] N. B. Jørgensen, L. Wacker, K. T. Skalmstang, M. M. Parish, J. Levinsen, R. S. Christensen, G. M. Bruun, and J. J. Arlt, *Phys. Rev. Lett.* **117**, 055302 (2016).
- [6] M.-G. Hu, M. J. de Graaff, D. Kedar, J. P. Corson, E. A. Cornell, and D. S. Jin, *Phys. Rev. Lett.* **117**, 055301 (2016).
- [7] L. A. Peña Ardila, N. B. Jørgensen, T. Pohl, S. Giorgini, G. M. Bruun, and J. J. Arlt, *Phys. Rev. A* **99**, 063607 (2019).
- [8] Z. Z. Yan, Y. Ni, C. Robens, and M. W. Zwierlein, *Science* **368**, 190 (2020).
- [9] M. G. Skou, T. G. Skov, N. B. Jørgensen, K. K. Nielsen, A. Camacho-Guardian, T. Pohl, G. M. Bruun, and J. J. Arlt, *Nature Physics* **17**, 731 (2021).
- [10] P. Massignan and G. M. Bruun, *Eur. Phys. J. D* **65**, 83 (2011).
- [11] R. Schmidt, M. Knap, D. A. Ivanov, J.-S. You, M. Cetina, and E. Demler, *Reports on Progress in Physics* **81**, 024401 (2018).
- [12] F. Scazza, M. Zaccanti, P. Massignan, M. M. Parish, and J. Levinsen, *Atoms* **10**, 10.3390/atoms10020055 (2022).
- [13] R. S. Lous, I. Fritsche, M. Jag, F. Lehmann, E. Kirilov, B. Huang, and R. Grimm, *Physical Review Letters* **120**, 10.1103/physrevlett.120.243403 (2018).
- [14] G. Ness, C. Shkredov, Y. Florshaim, O. K. Diessel, J. von Milczewski, R. Schmidt, and Y. Sagi, *Phys. Rev. X* **10**, 041019 (2020).
- [15] C. J. Vale and M. Zwierlein, *Nature Physics* **17**, 1305 (2021).
- [16] M. Tomza, K. Jachymski, R. Gerritsma, A. Negretti, T. Calarco, Z. Idziaszek, and P. S. Julienne, *Rev. Mod. Phys.* **91**, 035001 (2019).
- [17] C. Franchini, M. Reticcioli, M. Setvin, and U. Diebold, *Nature Reviews Materials* **6**, 756 (2021).
- [18] U. Bissbort, D. Cocks, A. Negretti, Z. Idziaszek, T. Calarco, F. Schmidt-Kaler, W. Hofstetter, and R. Gerritsma, *Phys. Rev. Lett.* **111**, 080501 (2013).
- [19] R. S. Lous and R. Gerritsma, in [Advances In Atomic, Molecular, and Optical Physics](#) (Elsevier, 2022) pp. 65–133.
- [20] K. Kleinbach, F. Engel, T. Dieterle, R. Löw, T. Pfau, and F. Meinert, *Physical Review Letters* **120**, 193401 (2018-05).
- [21] T. Feldker, H. Fürst, H. Hirzler, N. V. Ewald, M. Mazzanti, D. Wiater, M. Tomza, and R. Gerritsma, *Nature Physics* **16**, 413 (2020).
- [22] T. Dieterle, M. Berngruber, C. Hölzl, R. Löw, K. Jachymski, T. Pfau, and F. Meinert, *Physical Review Letters* **126**, 033401 (2021-01).
- [23] C. Veit, N. Zuber, O. Herrera-Sancho, V. Anasuri, T. Schmid, F. Meinert, R. Löw, and T. Pfau, *Physical Review X* **11**, 011036 (2021-02).
- [24] M. Drescher, M. Salmhofer, and T. Enss, *Phys. Rev. A* **99**,

- 023601 (2019).
- [25] L. A. P. n. Ardila, *Phys. Rev. A* **103**, 033323 (2021).
- [26] P. Weckesser, F. Thielemann, D. Wiater, A. Wojciechowska, L. Karpa, K. Jachymski, M. Tomza, T. Walker, and T. Schaeztz, *Nature* **600**, 429 (2021-12).
- [27] R. Côté, V. Kharchenko, and M. D. Lukin, *Phys. Rev. Lett.* **89**, 093001 (2002).
- [28] P. Massignan, C. J. Pethick, and H. Smith, *Phys. Rev. A* **71**, 023606 (2005).
- [29] J. M. Schurer, A. Negretti, and P. Schmelcher, *Phys. Rev. Lett.* **119**, 063001 (2017).
- [30] W. Casteels, J. Tempere, and J. T. Devreese, *Journal of Low Temperature Physics* **162**, 266 (2011).
- [31] G. E. Astrakharchik, L. A. P. Ardila, R. Schmidt, K. Jachymski, and A. Negretti, *Communications Physics* **4**, 10.1038/s42005-021-00597-1 (2021-05).
- [32] E. R. Christensen, A. Camacho-Guardian, and G. M. Bruun, *Phys. Rev. Lett.* **126**, 243001 (2021).
- [33] E. R. Christensen, A. Camacho-Guardian, and G. M. Bruun, *Physical Review A* **105**, 023309 (2022-02).
- [34] K. Myśliwy and K. Jachymski, The long-range interacting fermi polaron (2023), [arXiv:2310.04351](https://arxiv.org/abs/2310.04351) [cond-mat.quant-gas].
- [35] J. Pérez-Ríos, *Molecular Physics* **119**, e1881637 (2021), <https://doi.org/10.1080/00268976.2021.1881637>.
- [36] F. Chevy, *Phys. Rev. A* **74**, 063628 (2006).
- [37] M. Krych and Z. Idziaszek, *Phys. Rev. A* **91**, 023430 (2015).
- [38] R. Pessoa, S. A. Vitiello, and L. A. P. Ardila, *Physical Review A* **104**, 043313 (2021-10).
- [39] The mean-field energy corresponds to the limit  $b \gg r_*$ , however it can be also recovered from first-order perturbation theory  $E^{\text{MF}} = nV(\mathbf{k} = \mathbf{0})$  being  $V(\mathbf{k})$  the Fourier transform of the ion-atom potential.
- [40] M. Punk, P. T. Dumitrescu, and W. Zwerger, *Phys. Rev. A* **80**, 053605 (2009).
- [41] M. M. Parish and J. Levinsen, *arXiv e-prints*, [arXiv:2306.01215](https://arxiv.org/abs/2306.01215) (2023), [arXiv:2306.01215](https://arxiv.org/abs/2306.01215) [cond-mat.quant-gas].
- [42] R. Schmidt and T. Enss, *SciPost Phys.* **13**, 054 (2022).
- [43] T. Dieterle, M. Berngruber, C. Hölzl, R. Löw, K. Jachymski, T. Pfau, and F. Meinert, *Phys. Rev. A* **102**, 041301 (2020).
- [44] S. Nascimbène, N. Navon, K. J. Jiang, L. Tarruell, M. Teichmann, J. McKeever, F. Chevy, and C. Salomon, *Physical Review Letters* **103**, 170402 (2009-10).
- [45] S. Ding, M. Drewsen, J. J. Arlt, and G. M. Bruun, *Phys. Rev. Lett.* **129**, 153401 (2022).
- [46] G. E. Astrakharchik, L. A. P. Ardila, K. Jachymski, and A. Negretti, *Nature Communications* **14**, 1647 (2023).
- [47] A. J. Campbell, M. Brotons-Gisbert, H. Baek, V. Vitale, T. Taniguchi, K. Watanabe, J. Lischner, and B. D. Gerardot, *npj 2D Materials and Applications* **6**, 79 (2022).
- [48] D. K. Efimkin, E. K. Laird, J. Levinsen, M. M. Parish, and A. H. MacDonald, *Phys. Rev. B* **103**, 075417 (2021).
- [49] G. F. Gribakin and V. V. Flambaum, *Physical Review A* **48**, 546 (1993-07).
- [50] R. D. P. Szymtowski, *Acta Physica Polonica A* **79**, 613 (1991).
- [51] M. Sroczynska and Z. Idziaszek, *Physical Review A* **102**, 063312 (2020-12).
- [52] V. R. Pandharipande and K. E. Schmidt, *Phys. Rev. A* **15**, 2486 (1977).
- [53] J. Carlson, S.-Y. Chang, V. R. Pandharipande, and K. E. Schmidt, *Phys. Rev. Lett.* **91**, 050401 (2003).
- [54] S. Y. Chang, V. R. Pandharipande, J. Carlson, and K. E. Schmidt, *Physical Review A (Atomic, Molecular, and Optical Physics)* **70**, 043602 (2004).
- [55] D. M. Ceperley and M. H. Kalos, in *Monte Carlo Methods in Statistics Physics*, Topics in Current Physics, Vol. 7, edited by K. Binder (Springer-Verlag, Berlin, 1986) 2nd ed., Chap. Quantum Many-Body Problems, pp. 145–194.
- [56] P. J. Reynolds, D. M. Ceperley, B. J. Alder, and W. A. Lester, *J. Chem. Phys.* **77**, 5593 (1982).
- [57] J. W. Moskowitz, K. E. Schmidt, M. A. Lee, and M. H. Kalos, *J. Chem. Phys.* **77**, 349 (1982).
- [58] R. Bombín, T. Comparin, G. Bertaina, F. Mazzanti, S. Giorgini, and J. Boronat, *Physical Review A* **100**, 10.1103/physreva.100.023608 (2019).
- [59] A. B. Migdal, *Journal of Experimental and Theoretical Physics* **32**, 399 (1957).
- [60] J. Vlietinck, J. Ryckebusch, and K. V. Houcke, *Physical Review B* **87**, 115133 (2013).

**SUPPLEMENTAL MATERIAL FOR "FERMI POLARON IN AN ATOM-ION HYBRID SYSTEMS"**

Renato Pessoa,<sup>1</sup> Silvio Vitiello,<sup>2</sup> and Luis A. Peña Ardila,<sup>3</sup>

<sup>1</sup> Instituto de Física, Universidade Federal de Goiás - UFG, 74001-970 Goiânia, GO, Brazil

<sup>2</sup>Instituto de Física Gleb Wataghin, Universidade Estadual de Campinas - UNICAMP, 13083-970 Campinas, SP, Brazil

<sup>3</sup> School of Science and Technology, Physics Division, University of Camerino, Via Madonna delle Carceri, 9B - 62032 (MC), Italy

This supplementary material describes details on the two-body problem for the atom-ion interaction potential, employing the Buckingham polarization potential model where analytical expression can be derived for the  $s$ -wave scattering length. In addition, we include the most relevant systematic and technical aspects of the variational (VMC) and diffusion quantum Monte Carlo (DMC) methods. Specifically, we discuss the detailed functional forms of our trial wave functions and the estimators employed for the rigorous characterization of ground-state properties.

### I. THE ATOM-ION INTERACTION

The interaction between a neutral atom and a positive charged particle is given by [16]

$$V_{\text{ai}}(\mathbf{r}) = -\frac{C_4}{r^4}. \quad (\text{S1})$$

The strength of this potential  $C_4 = \alpha e^2/2$  depends on the static polarisability  $\alpha$  of the atom and  $e$  is the elementary electrostatic charge. The electrostatic forces, even playing an important role in the behavior of the system, are not sufficient to fully describe the atom-ion interaction. At short ranges, the exact form of the potential is complex and generally unknown, and the  $V_{\text{ai}}$  potential is singular as  $r \rightarrow 0$ . A common approach [31, 33] to address these difficulties is provided by a convenient regularization of this potential [37],

$$V_{\text{ai}}^r(\mathbf{r}) = -C_4 \frac{r^2 - c^2}{r^2 + c^2} \frac{1}{(b^2 + r^2)^2}, \quad (\text{S2})$$

where  $b$  and  $c$  are parameters chosen to describe the low energy properties of the system. The cut-off radius  $b$  deepens the modeled potential as its value is decreased, while  $c$  sets the distance at which the interaction becomes repulsive, to avoid overlap of the electronic wavefunctions of the atom-ion dimer. The pair  $(b, c)$  parameters draw the two-body energy spectrum of the system parametrized by the atom-ion scattering length. Additionally, the regularized potential energy has a finite value as  $r \rightarrow 0$ , a useful feature in many numerical calculations.

For the alkali atoms, the characteristic length is  $r_* \sim \mathcal{O}(10^3)$  Å, and in this work, the value  $c = 0.0023r_*$  is used. Changing the parameter  $b$  tunes the energy of the bound state, mimicking experiments where Feshbach resonances have recently been observed [26]. From a two-body level, we determine the values of  $b$  at which the dissociation of bound states of the atom-ion occurs by solving the Schrödinger equation for the zero-energy limit. Namely,

$$\left[ \frac{d^2}{dr^2} + \frac{r^2 - c^2}{r^2 + c^2} \frac{1}{(b^2 + r^2)^2} \right] \psi(r) = 0. \quad (\text{S3})$$

To obtain the values of  $b$  for dissociation, the wave function must satisfy the boundary conditions  $\psi(0) = 0$  and  $\psi'(0) = \epsilon$  at the origin, where  $\epsilon$  is any small number. The  $s$ -wave scattering length is determined by iteratively solving the radial time-independent Schrödinger equation of Eq. (S3) for different values of  $b$ . The solution for the radial function,  $\chi(r) = \psi(r)/r$ , can be found by matching the semiclassical wave function in the attractive part of the interaction with the asymptotic exact solution using the  $-1/r^4$  potential [49]. It is possible to assume that as  $r \rightarrow \infty$ , the potential approaches zero, leading to

$$\chi(r) \underset{r \rightarrow \infty}{\sim} A(r - a), \quad (\text{S4})$$

where  $A$  is a constant and  $a$  is the scattering length for the  $s$ -wave zero-energy. The scattering length exhibits resonances as  $b$  decreases, each one corresponding to the appearance of a deeper bound state.

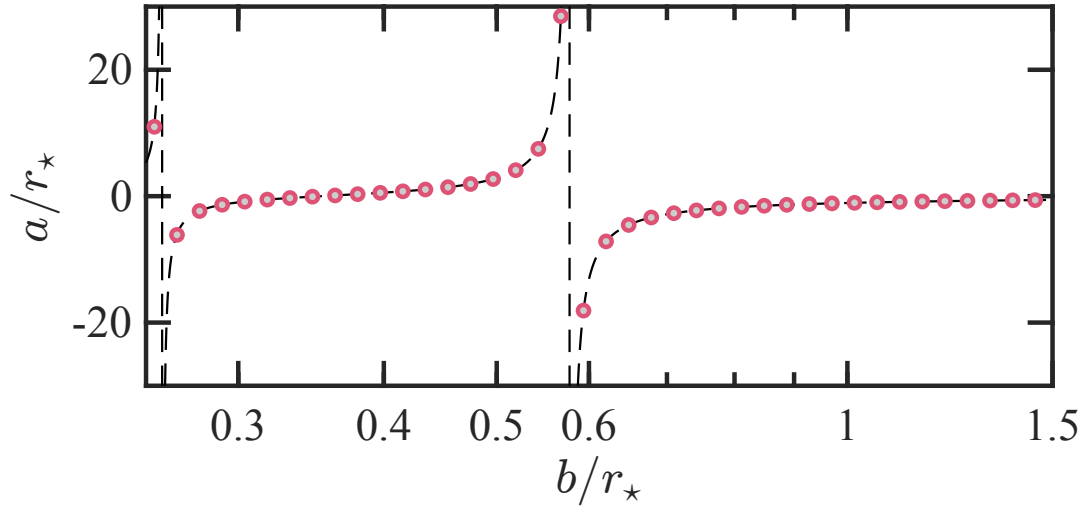


FIG. S1. Numerical solution of the atom-ion scattering length as a function of the parameter  $b$  and  $c = 0.0023r_*$  (red circles) and exact result Eq. S5.

We can confirm that the constant prefactor dependent on  $c$  in the regularized potential described by Eq. (S2), responsible for its short-range behavior, can be safely ignored in this work by considering the Buckingham polarization potential. This potential is obtained when the approximation  $(r^2 - c^2)/(r^2 + c^2) \approx 1$  is valid. In this case, the Schrödinger equation can be solved analytically and the scattering length can be expressed as [50, 51]

$$a = (1 + b^2)^{1/2} \cot \frac{\pi}{2} (1 + b^{-2})^{1/2}. \quad (\text{S5})$$

In Fig. S1, we superimpose the scattering lengths of Eq. (S5) with those obtained by iteratively solving the zero-energy Schrödinger equation with the full regularized potential of Eq. (S2). The agreement between the two is excellent.

## II. QUANTUM MONTE CARLO DETAILS

The wave function model used in the simulations is of Jastrow-Slater form,

$$\psi_T(R) = \prod_i f(r_{i\downarrow}) D_{\uparrow} e^{i\mathbf{k}\cdot\mathbf{r}_{\downarrow}}, \quad (\text{S6})$$

where  $R \equiv \{\mathbf{r}_1, \dots, \mathbf{r}_N, \mathbf{r}_{\downarrow}\}$  represents the space points of all the atoms, and  $D_{\uparrow}$  is a Slater determinant for the up-spin particles. The single particle orbitals are chosen to be plane waves. Wave vectors are given by  $k = \frac{2\pi}{L} \sqrt{n_x^2 + n_y^2 + n_z^2}$  where  $n_x, n_y$  and  $n_z$  are positive or negative integers and  $L$  is the side of the simulation box. In this way,

$$D_{\uparrow} = \mathcal{A} \prod_j e^{i\mathbf{k}\cdot\mathbf{r}_j} \quad (\text{S7})$$

where  $\mathcal{A}$  is an antisymmetrizer operator. Most calculations considers closed shells for the up-spin bath, where the number of particles is defined by the maximum value of  $I = n_x^2 + n_y^2 + n_z^2$ . For example, for the bath with  $N = 81$  particles, we have  $I_{\max} = 6$  to take into account the closed shells case.

The form of the Jastrow term  $f(r)$ , in the trial wave function, depends on the value of  $b$ . For  $b/r_* > 0.58$  the lowest-order constrained variational (LOCV) method [52–54] is employed to obtain  $f(r)$ . This involves solving the two-body Schrödinger like equation

$$\left[ -\frac{\hbar^2}{2\mu} \nabla^2 + V(r) \right] f(r) = \lambda f(r), \quad (\text{S8})$$

where the  $\lambda$  parameter is chosen to ensure the continuity of  $f(r)$ . Specifically,  $\frac{df}{dr} = 0$  for  $r = \mathcal{D}$ , and it is imposed that  $f(r \geq \mathcal{D}) = 1$ ;  $\mathcal{D}$  is the range of the Jastrow term. The value of the  $\mathcal{D}$  parameter is obtained by minimizing the value of the energy in the VMC as explained further below.



For  $b/r_* < 0.58$ , the interatomic potential becomes deeper and it is important to consider a phononic contribution in the wave function. The Jastrow factor obtained from Eq. (S8) is modified by adding a tail

$$A \exp \left[ -C \left( \frac{1}{L-r} + \frac{1}{r} \right) \right] \quad (\text{S9})$$

for  $\bar{r} \leq r \leq L/2$ , where  $\bar{r}$  is a variational parameter chosen to minimize the trial energy. Parameters  $A$  and  $C$  are chosen to ensure continuity of the wave function at the distance  $\bar{r}$  and in the simulation box boundary. Simulations considering the phononic contribution have shown that for large enough values of  $\mathcal{D}$  its value is not critical, we have adopted  $\mathcal{D} = L/2$ .

The VMC method involves sampling the probability distribution

$$p(R) = \frac{|\psi_T(R)|^2}{\int dR |\psi_T(R)|^2}, \quad (\text{S10})$$

where  $\psi_T(R)$  is the trial wave function. The variational energy is estimated by approximating the integral  $\int dR p(R) E_L(R)$  by the average values of the local energy  $E_L(R) = H\psi_T/\psi_T(R)$  over the sampled configurations [55]. The aim of VMC in this work is to optimize the variational parameters entering the trial wave functions.

The DMC method solves the Schrödinger equation for imaginary time  $\tau$

$$-\frac{\partial \Psi}{\partial \tau} = (H - E_T)\Psi, \quad (\text{S11})$$

where  $E_T$  is a constant. Importance sampling is required for the system to explore the most important regions of the configuration space. Through this transformation, converged samples are drawn from the distribution  $\psi_0\psi_G$ , where  $\psi_G$  is the trial wave function  $\psi_T$ . The Hermiticity of the system Hamiltonian allows for an unbiased estimation of energy in systems following Bose-Einstein statistics by averaging the local energy. However, estimation of any quantity  $Q$  that does not commute with the Hamiltonian requires extrapolation  $Q_{\text{extr}} = 2Q_{\text{DMC}} - Q_{\text{VMC}}$ , which depends on a variational  $Q_{\text{VMC}}$  result.

Simulations are carried out by considering the fixed-node approximation to avoid the sign problem, a change in the sign problem when one particle crosses the nodal surface of the guiding function [56, 57]. In the simulations, to guarantee results free from time step bias, the value of the time step was carefully analyzed by verifying that the energy of an impurity in a bath of  $N = 123$  particles did not change for  $\Delta\tau = 10^{-4}$ ,  $\Delta\tau = 2 \times 10^{-4}$  and  $\Delta\tau = 5 \times 10^{-4}$ . The value  $\Delta\tau = 10^{-4}$  was chosen to avoid a move where a particle crosses more than one nodal hyper-surface and reaches a region with the original sign, the cross-recross error.

The wave function associated with the polaron is constructed following the Jastrow-Slater model described in Eq. (S6) where the momentum states of the up-spin particles of the bath are fully occupied for  $I \leq I_{\text{max}}$ . On the other hand, the wave function for the molecular case has a different nodal structure that emerges from changes made in the Slater determinant. In this case, the down-spin impurity is set in the first momentum state above the Fermi state. Furthermore, a bath particle is removed from the highest filled momentum state and set in the same ion impurity momentum state. As observed in Fig.2 in the main text, in the neighborhood of the resonance of the two nodal surfaces match despite the molecular nodal surface imposed in the trial wave function should favor the molecule over the polaron. In Fig. S2 we have extended further the parameter window of  $b$  to observe that the polaron and molecular branch are essentially indistinguishable within statistical error.

The polaron energy is estimated by subtracting from a simulation with one ion in the momentum state with  $k = 0$  and the pure system formed by the bath (as defined in the main text)

$$\mu = E^0(N_\uparrow, 1_\downarrow) - \frac{3}{5}N_\uparrow\epsilon_F. \quad (\text{S12})$$

Although  $\epsilon_F$  is known exactly,  $\mu$  is not an easy quantity to estimate. The long-range character of the interatomic interaction requires large systems, *i.e.*, a large number of particles in the bath, that tend to mask the contribution of the impurity in the uncertainty of the simulation result. This situation prompts a careful consideration of size effects in the results as for instance, panel (a) in Fig. S2.

The effective mass  $m^*$  of the ionic Fermi polaron obtained for the model of quasiparticle is given by

$$E_p(\mathbf{p}) \sim \frac{\mathbf{p}^2}{2m^*} + \mu, \quad (\text{S13})$$

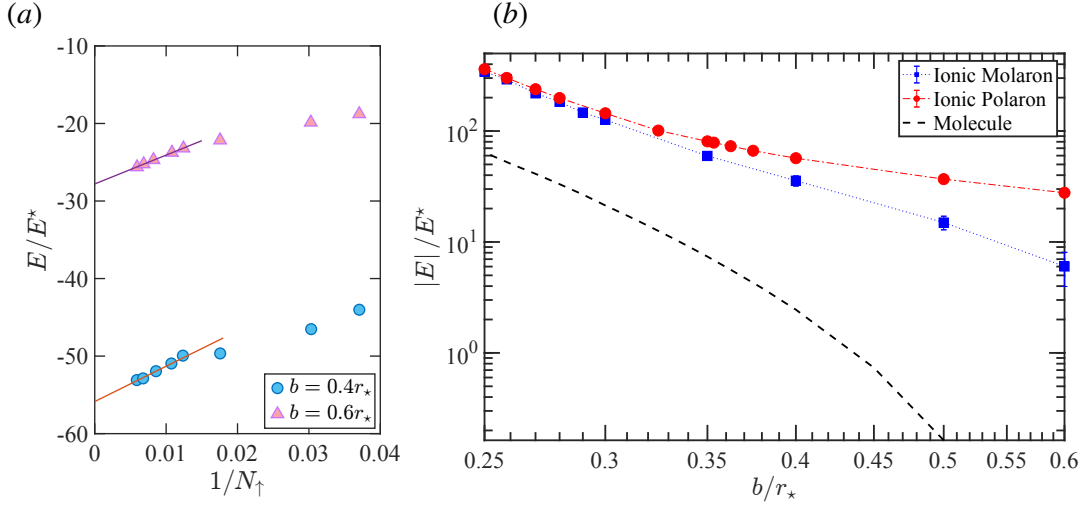


FIG. S2. (a) Typical size effect for the energy at zero momentum for two values of the atom-ion potential. (b) Polaron energy of the attractive polaron ( $E_p$ ) and the molecular polaron "molaron" ( $E_M$ ) in the neighborhood of the resonance. The same parameters are from Fig. 2 in the main text.

where  $\mathbf{p} = \hbar\mathbf{k}$  is the impurity momentum and  $\varepsilon$  the ground state polaron energy. We extracted this quantity by placing the impurity in the first three states available in three different simulations. Finally, by plotting  $E_p(\mathbf{k})$  as a function of  $k^2$ , with a fit to the results, the effective mass was obtained. A different method was used in Ref. [58] where this quantity could be obtained in a single run by considering the imaginary time displacement of the impurity.

At zero temperature, an ideal Fermi gas has all its lowest energy levels filled. The introduction of an impurity induces low-energy excitations, which might result in quasiparticles. The Migdal theorem [59] asserts the existence of a discontinuity in the momentum distribution  $n(k)$  at the Fermi momentum  $k_F$  of the ion, characterizing the residue  $Z$ . This residue is calculated as the difference between the momentum distribution,

$$Z = n(k_F - \delta) - n(k_F + \delta), \quad (\text{S14})$$

where  $\delta$  is an infinitesimal positive constant. In the thermodynamic limit,  $n(k_F + \delta)$  approaches zero due to the scaling of the associated one-body density matrix with the system volume. Consequently, the residue  $Z$  can be identified with the momentum distribution at  $k_F$  of the ion. An estimator for  $Z$  is obtained from the one-body density matrix

$$Z = \lim_{|\mathbf{r}'_\downarrow - \mathbf{r}_\downarrow| \rightarrow \infty} \left\langle \frac{\psi(R')}{\psi(R)} \right\rangle \quad (\text{S15})$$

where  $R' \equiv \{\mathbf{r}_1, \dots, \mathbf{r}_N, \mathbf{r}'_\downarrow\}$  represents space points for atoms in the bath, and  $\mathbf{r}'_\downarrow$  represents an arbitrary displacement of the impurity. A non-zero residue characterizes the polaron as a quasiparticle, indicating the overlap between the ground state wave function of the non-interacting (impurity and free gas) and the interacting system [58, 60].

### III. INFINITE MASS CASE

One possibility to reduce micromotion and characterize the Fermi polarons is to consider the regime of heavy impurities. In Fig. S3 we estimate the polaron energy and the quasiparticle residue for the relevant experimental case  $^{176}\text{Yb}^+ - ^6\text{Li}$  which corresponds to the mass ratio,  $m_I/m_F \sim 30$ . The polaron energy is plotted for two densities,  $nr_*^3 = 0.1$  and  $nr_*^3 = 1$ . In the former case and for  $b \gg r_*$  the results are compatible with the mean-field result for the heavy Fermi polaron,  $E = -\pi^2 \frac{n}{b} \frac{\hbar^2}{2\mu r_*^2}$ .

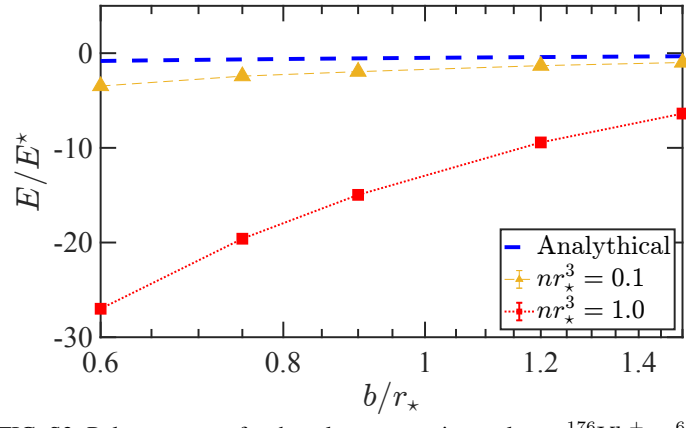


FIG. S3. Polaron energy for the relevant experimental case  $^{176}\text{Yb}^+ - ^6\text{Li}$